

# Optimal Material Properties of Molding Compounds for MEMS Package

Yeonsung Kim, Hohyung Lee, Xin Zhang, and Seungbae Park

**Abstract**—In this paper, an optimization study of molding compounds for a microelectromechanical systems (MEMS) sensor package has been performed. A comprehensive finite element analysis model was established for the MEMS sensor package to assess the stresses and deformations when the package was subjected to temperature loading. A series of stress relaxation tests were performed to characterize the viscoelastic material properties of a molding compound over temperature with dynamic mechanical analysis. A master curve for the molding compound was constructed by a proper shift function and the Prony pairs were obtained by curve fitting to be implemented in the simulation. To validate the simulation result, the thermal behavior of the MEMS package was measured. The digital image correlation technique was employed to observe the real-time deformation of the package exposed to temperature loading. The out-of-plane deformation of the package was compared with the simulation result. With the validated simulation model, the optimization study was conducted. By the process simulation, it has been shown that most of the thermal stress on the MEMS sensor chip was generated during the cooling process. Thus, a detailed cooling profile was developed by the transient heat analysis and applied to the parametric study. The modulus, coefficient of thermal expansion (CTE), and glass transition temperature ( $T_g$ ) of molding compound were investigated. The result shows that a low modulus, low CTE, and low  $T_g$  molding compound can minimize the thermal stress on MEMS sensor die.

**Index Terms**—Master curve, microelectromechanical systems (MEMS), molding compound, relaxation modulus, viscoelasticity.

## I. INTRODUCTION

**M**ICROELECTROMECHANICAL systems (MEMS) sensor devices are widely used in electronics to measure displacement, acceleration, pressure, and so on. The output of the MEMS sensor is, however, often disturbed by thermomechanical and mechanical stresses since the MEMS structure is highly sensitive to the stress. The shift of initial null point of output by stress results in lowering the accuracy and degrading the performance of the MEMS sensor [1], [2]. The MEMS packages consist of various

materials that have different thermomechanical properties. A discrepancy in material properties of component materials induces the internal stresses acting on sensor device during assembly process and under thermal cycling by operation. Thus, it is essential to understand the thermomechanical stress development and change during the manufacturing process and temperature cycle of MEMS sensor package to ensure its accuracy and reliability. The MEMS sensor products are usually encapsulated by plastic molding compound to protect the sensor die from the environment. One of the most distinguishing characteristics of the plastic molding compound is viscoelasticity. Polymer-based material such as plastic molding compound exhibits an intermediate behavior between a solid and a liquid. Due to the viscoelasticity, plastic molding compounds show both temperature and time-dependent behavior. Since the plastic molding compound comprises a significant portion of the MEMS sensor package, the viscoelasticity should be considered for more accurate estimation of stresses and strains inside the package.

Molding compound effects on packaging stress and warpage has been one of the critical issues in the microelectronics industry. Amagai [3] characterized the molding compound to enhance solder joint reliability and warpage of CSP. Srikanth [4] investigated warpage of package during cooling process after the molding. Tsai *et al.* [5] studied the molding compound-induced residual/thermal deformation and stress in plastic IC packages during the fabrication processes. Alpern *et al.* [6] reported metal deformation and passivation crack of chip due to molding compound. To implement viscoelastic material properties of molding compound in finite element analysis (FEA), characterization study was performed in [7]. However, compared with the papers addressing the packaging and thermal stress for other ICs, not many papers have been published so far for MEMS sensor devices. Zhang *et al.* [1], Rudolf and Kim [2], and Krondorfer *et al.* [8] reported papers on packaging stress of MEMS sensors and its effect on device offset to increase the performance. Joo and Choa [9] measured the real-time deformation of MEMS gyroscope sensor subjected to temperature change using moiré interferometry. In spite of the sensitivity of MEMS sensor devices, optimization studies about molding compound viscoelasticity for MEMS are still absence.

In this paper, the effects of the molding compound material properties on MEMS device stress was investigated by FEA. The deformation of sensor die was observed to evaluate the effect of molding compound during a given temperature

Manuscript received September 20, 2013; revised March 25, 2014; accepted August 6, 2014. Date of publication September 7, 2014; date of current version October 3, 2014. Recommended for publication by Associate Editor K. N. Chiang upon evaluation of reviewers' comments.

Y. Kim, H. Lee, and S. Park are with the Department of Mechanical Engineering, State University of New York at Binghamton, Binghamton, NY 13850 USA (e-mail: ykim35@binghamton.edu; hlee11@binghamton.edu; sbpark@binghamton.edu).

X. Zhang is with the MEMS/Sensors Products and Technologies Group, Analog Devices Inc., Wilmington, MA 01887 USA (e-mail: sam.zhang@analog.com).

Color versions of one or more of the figures in this paper are available online at <http://ieeexplore.ieee.org>.

Digital Object Identifier 10.1109/TCPMT.2014.2351574

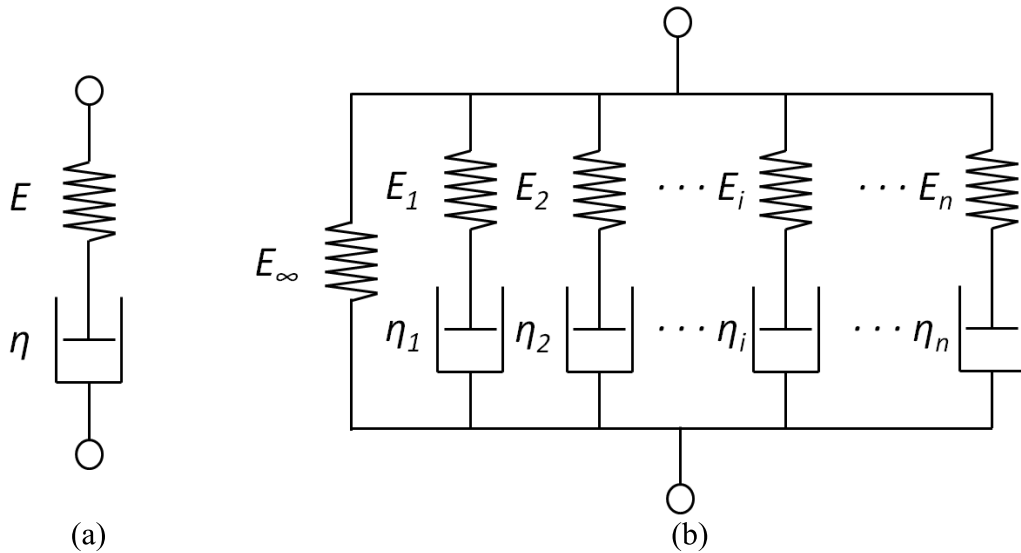


Fig. 1. Models to describe the viscoelastic behavior. (a) Maxwell model. (b) Generalized Maxwell model.

and time profile. The viscoelasticity of molding compound was characterized by the stress relaxation test using dynamic mechanical analysis (DMA) and the master curve was obtained by the proper shift function. To model the viscoelasticity using FEA, the master curve was fitted with Prony function. To verify the simulation results, the real-time deformation of MEMS device exposed to thermal loading was monitored by digital image correlation (DIC). The validation between the out-of-plane deformation of MEMS device by DIC and FEA was carried out. Then, optimization study was conducted with the validated FEA model. The simulation was performed to investigate the stress development and warpage change of the MEMS sensor die during the assembly process. The cooling profile from the postmold cure (PMC) temperature to room temperature was obtained by transient analysis and subsequently utilized in the optimization simulation. The optimization study was assessed in terms of stress of sensor die. The influence of modulus, coefficient of thermal expansion (CTE), and  $T_g$  of molding compound on sensor chip stress was studied in detail.

## II. VISCOELASTICITY AND TIME-TEMPERATURE SUPERPOSITION

Viscoelastic materials are in the intermediate state between solid and liquid that possesses both elastic and viscous characteristics. The viscoelastic behavior can be expressed with Hookean springs and Newtonian dashpot, which correspond to pure elastic and pure viscous property, respectively. Due to the viscosity, viscoelastic materials exhibit both time and temperature-dependent properties. To measure this characteristic of the viscoelastic material, stress relaxation, or creep tests are often implemented. The Maxwell model is commonly used to describe stress relaxation of viscoelastic materials. Fig. 1(a) shows the Maxwell element and the behavior of this model can be expressed as

$$\sigma(t) = E\varepsilon \exp\left(-\frac{t}{\tau}\right), \quad \tau = \frac{\eta}{E} \quad (1)$$

where  $\sigma(t)$  is the stress as a function of time,  $E$  is the elastic modulus,  $\eta$  is the material coefficient of viscosity, and  $\tau$  is a time constant. This model illustrates a single relaxation time. A generalized Maxwell model shown in Fig. 1(b), which consists of a number of Maxwell elements connected in parallel, is used to approximate the real behavior of a viscoelastic material. Each spring and dashpot has their own elastic modulus and viscosity. Such a system can be modeled as

$$\sigma(t) = \varepsilon_0 \left[ E_\infty + \sum_{i=1}^n E_i \exp\left(-\frac{t}{\tau_i}\right) \right]. \quad (2)$$

Here,  $i$  represents the number of number of elements connected in parallel,  $E_i$  is the modulus of the  $i$ th element,  $\varepsilon_0$  is the imposed strain at  $t = 0$ , and  $E_\infty$  is the fully-relaxed modulus. Finally, the relaxation modulus can be expressed as

$$E(t) = \frac{\sigma(t)}{\varepsilon_0} = E_\infty + \sum_{i=1}^n E_i \exp\left(-\frac{t}{\tau_i}\right). \quad (3)$$

This representation is called the Prony series. In this equation,  $E_i$  and  $\tau_i$  are referred to as a Prony pair, which is used in many simulation software tools to describe the viscoelasticity. Based on the assumption of a thermorheologically simple material [7], time and temperature effects on viscoelastic materials can be accounted for using a simple curve known as the master curve. A single relaxation curve at a certain temperature merges with another relaxation curve at higher temperature after a certain amount of time. Thus, the master curve can be constructed by shifting relaxation curves at different temperatures along the log time scale axis. This is called time-temperature superposition. There are several functions to describe the shift distance. In this paper, a third-order polynomial shift function is adopted, which is expressed as

$$\log a_T(T) = C_1(T - T_0) + C_2(T - T_0)^2 + C_3(T - T_0)^3 \quad (4)$$

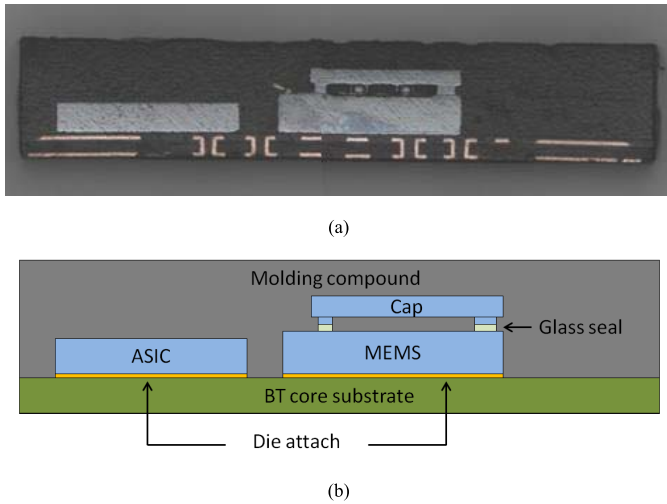


Fig. 2. MEMS sample. (a) Cross-sectional image. (b) Schematic view of MEMS.

where  $\alpha_T$  is a shift distance from the reference temperature of each relaxation curve at different temperature ( $T$ ),  $T_0$  is a reference temperature. The  $C_1$ ,  $C_2$ , and  $C_3$  are constants to be obtained from curve fitting.

### III. SAMPLE

The test vehicle used for this paper is shown in Fig. 2. The package is a land grid array type 3-axis accelerometer with dimensions of  $3 \text{ mm} \times 5 \text{ mm} \times 1 \text{ mm}$  ( $W \times L \times T$ ). The package consists of a MEMS die, an application specific integrated circuit (ASIC), substrate, and molding compound. The dimensions of the MEMS die is  $1.3 \text{ mm} \times 1.5 \text{ mm} \times 0.3 \text{ mm}$  and the ASIC is  $2.25 \text{ mm} \times 1.45 \text{ mm} \times 0.2 \text{ mm}$ . The thickness of the die attach adhesive is  $15\text{--}20 \mu\text{m}$ . The MEMS sensor is covered with a silicon cap to protect the MEMS structure. During the manufacturing processes, the MEMS die and ASIC are mounted on the substrate by die attach adhesive and wire-bonded, then finally encapsulated by the plastic molding compound. The process temperature of the die attach, wire bonding, and molding process is  $175 \text{ }^\circ\text{C}$ . The PMC condition is 4 h at  $175 \text{ }^\circ\text{C}$ .

### IV. EXPERIMENT

#### A. Stress Relaxation Test

Bar type test samples of the molding compound were fabricated by Analog Devices, Inc. The same PMC condition of the manufacturing process was applied. For the stress relaxation test, the samples were cut and polished into  $60 \text{ mm} \times 13 \text{ mm} \times 1 \text{ mm}$  ( $L \times W \times T$ ) bars. The DMA was chosen as the method to perform the stress relaxation test. The test was conducted in the three point bending mode. It is recommended to use the three point bending mode rather than the single cantilever loading mode due to the clamping effect, which usually results in an extracted value of relaxation modulus that is lower than the actual value. In addition, the surface of the molding compound bar was ground to be flat and uniform to achieve good alignment between the

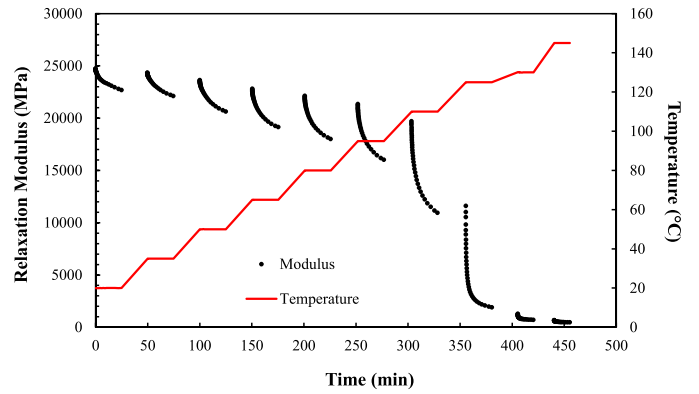


Fig. 3. Stress relaxation test result of molding compound.

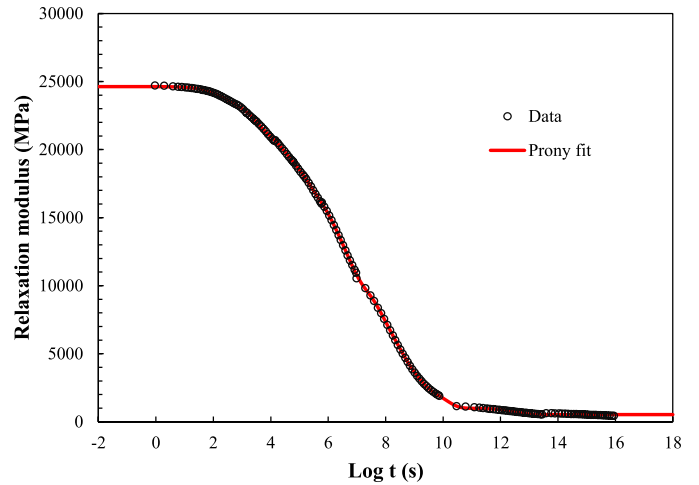


Fig. 4. Master curve from the stress relaxation test data and Prony fit by curve fitting program.

bending fixture and sample [10]. The stress relaxation test was conducted at  $15 \text{ }^\circ\text{C}$  intervals starting at  $20 \text{ }^\circ\text{C}$  and going up to  $125 \text{ }^\circ\text{C}$ , as well as at  $130 \text{ }^\circ\text{C}$  and  $145 \text{ }^\circ\text{C}$ . The ramp rate was  $5 \text{ }^\circ\text{C}/\text{min}$ . After waiting 5 min at the target temperature for temperature stabilization, a strain of  $0.02\%$  was applied for 15 min (10 min for  $130 \text{ }^\circ\text{C}$  and  $145 \text{ }^\circ\text{C}$ ), followed by a 10-min recovery time. The result is shown in Fig. 3.

To generate the master curve, the relaxation curves in Fig. 3 were plotted with respect to the log time scale. Then, the individual relaxation curves were shifted with respect to the reference temperature of  $20 \text{ }^\circ\text{C}$ . Fig. 4 shows the constructed master curve. To apply these viscoelastic properties in ANSYS, the Prony pairs of the master curve and shift function are required. Hence, the Prony series having 12 Prony pairs was programmed in a curve fitting program that was then fitted to the master curve. The Prony pairs from the curve fitting are listed in Table I. The solid line in Fig. 4 shows the Prony fit. Meanwhile, as previously mentioned, the third-order polynomial function was employed to fit the shift distance of the relaxation curves at various temperatures. There are common shift equations, such as Williams–Landel–Ferry and function in Arrhenius form (Tool–Naraswanaswamy function in ANSYS). Those functions usually choose  $T_g$  as the reference temperature. However, a better fit can be achieved

TABLE I  
PRONY PAIRS FOR THE MASTER CURVE OF MOLDING COMPOUND

$i$	$E_i$ (MPa)	$\tau_i$ (s)	$i$	$E_i$ (MPa)	$\tau_i$ (s)	$i$	$E_i$ (MPa)	$\tau_i$ (s)
$\infty$	526		5	2077	$9.4 \times 10^5$	10	860	$1.7 \times 10^2$
1	474	$4.0 \times 10^{12}$	6	1611	$1.3 \times 10^{10}$	11	2396	$4.7 \times 10^6$
2	1985	$2.5 \times 10^3$	7	1793	$2.1 \times 10^4$	12	2645	$5.4 \times 10^7$
3	2368	$4.7 \times 10^6$	8	2392	$1.4 \times 10^5$			
4	3024	$2.6 \times 10^8$	9	2478	$1.2 \times 10^9$			

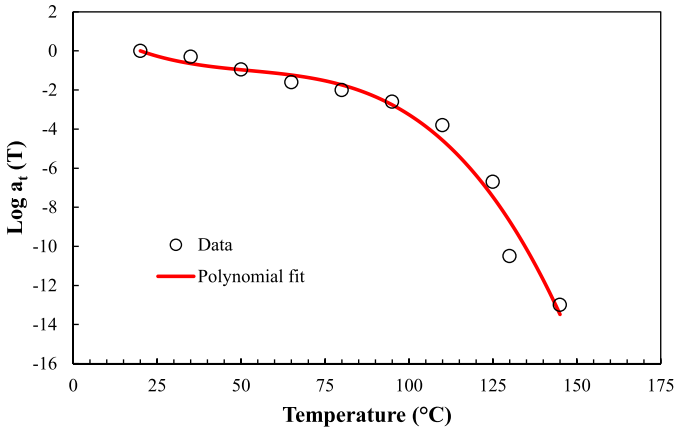


Fig. 5. Shift distance plot for the master curve with reference temperature of 20 °C and polynomial fit.

by a polynomial function regardless of  $T_g$  in many cases. The shift distance of individual relaxation curve and the third-order polynomial fit are shown in Fig. 5. The curve fitting program was also used to fit the shift distance. Three parameters of polynomial function were determined to be  $C_1 = 0.06034$ ,  $C_2 = -0.00136$ , and  $C_3 = 1.38822 \times 10^{-5}$ . Since ANSYS does not support the embedded polynomial function, a user-defined subroutine was used [11].

### B. CTE Measurement

The CTE of the molding compound was characterized by DIC. The DIC, which is a form of photogrammetry, is a non-contact, full-field optical measurement technique in which both the in-plane and out-of-plane displacement can be computed by pictures of the target object at the initial and deformed stage [15]. This is accomplished by correlating thousands of facets on the sample surface that act as strain gauges. The facets were generated on the sample surface by a white spray, and the experimental setup is shown in Fig. 6. The measurement resolution of the in-plane and out-of-plane displacement was about  $0.5 \mu\text{m}$ . By measuring in-plane deformation of the specimen, the material strain as a function of temperature can be obtained. The in-plane CTE is determined by taking the slope of the strain versus temperature graph. Fig. 7 shows the in-plane strain measurement result of the molding compound by DIC. The in-plane CTE of the molding compound is 9 ppm/°C below  $T_g$ , and 31 ppm/°C above  $T_g$ . The material properties used for FEA are listed in Table II.

### C. Out-of-Plane Deformation

The real-time deformation of MEMS under thermal loading was measured by DIC. Fig. 8 shows the profile of the thermal

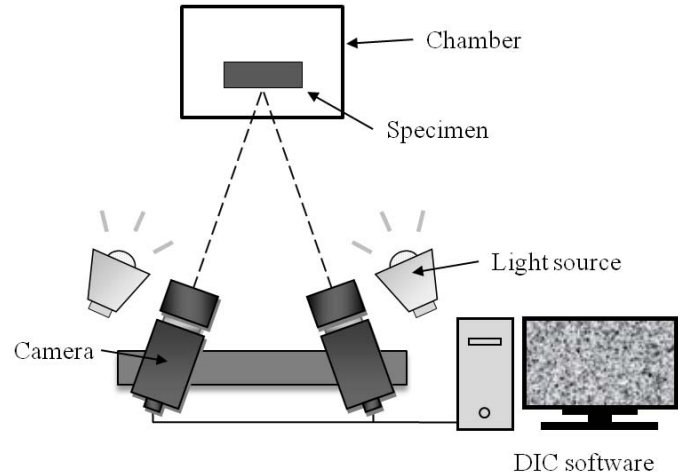


Fig. 6. 3-D DIC system setup.

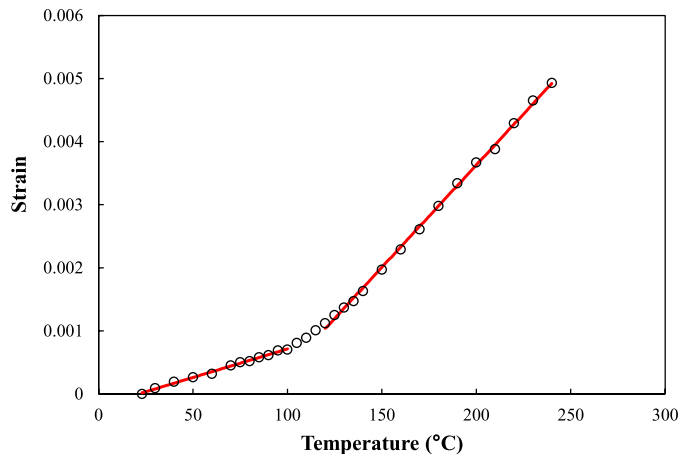


Fig. 7. In-plane thermal strain of molding compound.

loading used for the experiment. The thermal behavior of the package from room temperature to the reflow temperature was investigated. The mold side of the package was measured and the out-of-plane deformation data along a diagonal line was extracted to compare with the simulation. The result is shown in Fig. 9. Due to the letters etched on the mold surface, the smooth plot of out-of-plane deformation could not be obtained. In addition, it has to be noted that deformation at 25 °C was assumed to be zero. However, in the samples, initial deformation at room temperature may exist because of the cure shrinkage of molding compound after PMC process. During the PMC process, due to the polymerization of epoxy and fillers, the formation of highly cross-linked polymers results in a significant decrease in the specific volume [14]. However, the

TABLE II  
MATERIAL PROPERTIES

	E (GPa)	CTE (ppm/°C)	$T_g$ (°C)	$\nu$
Molding Compound	Table. 1	$\alpha$ 1 : 9 $\alpha$ 2 : 31	120	0.3
Si	163	2.6	-	0.22
Seal Glass	50	7	-	0.2
Solder Mask	2.4	$\alpha$ 1: 60 $\alpha$ 2: 130	100	0.3
Cu	129	16.5	-	0.35
Die Attach	0.24	129	0	0.4
BT Core	28	$\alpha$ 1 : 14 $\alpha$ 2 : 5	230	0.2

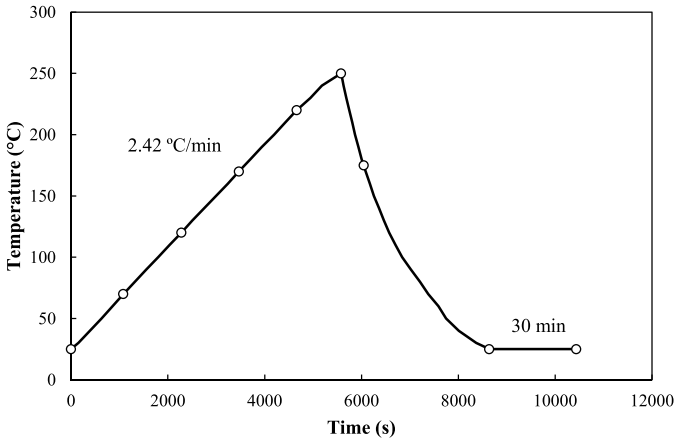


Fig. 8. Temperature profile for the out-of-plane deformation measurement.

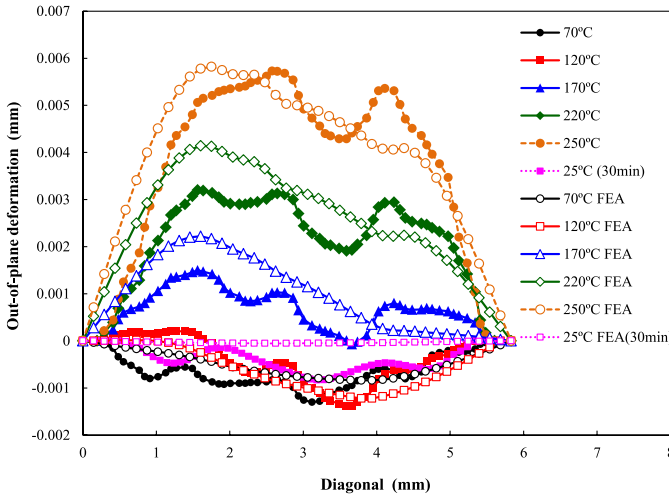


Fig. 9. Out-of-plane deformation of MEMS sensor device.

deformation caused by the cure shrinkage was not considered in this paper. The out-of-plane deformation relative to 25 °C was a parameter used to validate the simulation. After the measurement, the deformation of the sample was replotted with respect to 25 °C to remove the effect of cure shrinkage. This approach is valid because the cure shrinkage is an additional deformation and constant through the temperature change.

## V. SIMULATION

The ANSYS 14.5 was used to perform the simulation. Fig. 10 shows the FEA model for the MEMS sensor device. The model was mapped-meshed with a 3-D brick element (SOLID185). The XYZ displacement of bottom-left edge node, YZ displacement of bottom-right edge node, and Z displacement of top-right edge node on the bottom surface of the model were constrained as a boundary condition to remove rigid body motions. Since the temperature of the PMC process was 175 °C, this value was used as the reference (no deformation) temperature. The analysis started at 175 °C and the model was cooled to 25 °C in 1000 s, which corresponds to the end of the PMC process. Then, it was maintained at 25 °C for 9000 s (2.5 h) and then the simulation followed the thermal cycling profile in Fig. 8. The simulated warpage along the diagonal of the mold surface is shown in Fig. 9. Since the initial deformation (cure shrinkage effect) was already removed in the experimental result, the warpage curves from simulation were plotted with respect to 25 °C to compare the simulated and experimental results. As shown in Fig. 9, good agreement with experiment was obtained from the simulation. Based on this validation study, it can be concluded that even though there might be initial deformation, the warpage trend and travel distance in Z-axis can be predicted accurately with this model.

## VI. OPTIMIZATION STUDY

With the validated FEA model, a parametric study was conducted. In this experiment, the primary focuses were the stress of sensor chip. The  $\sigma_y$  at the center of the top surface of the sensor die was investigated because the in-plane stress of the sensor chip may worsen the performance of the MEMS device. The  $\sigma_x$  showed about 10% lower value than  $\sigma_y$  at the same point. First, the change of warpage and stress was investigated under the temperature profile mentioned previously. To observe the viscoelastic material effect, two types of models were analyzed. One model used the viscoelastic material property for molding compound and the other used a temperature-dependent elastic material property. In Fig. 3, the initial modulus of each stress relaxation test was used for the elastic modulus value at that temperature since the instantaneous modulus of stress relaxation test ( $t = 0$ ) should be identical with Young's modulus as seen in (1). The warpage change of sensor die is shown in Fig. 11. Compared with

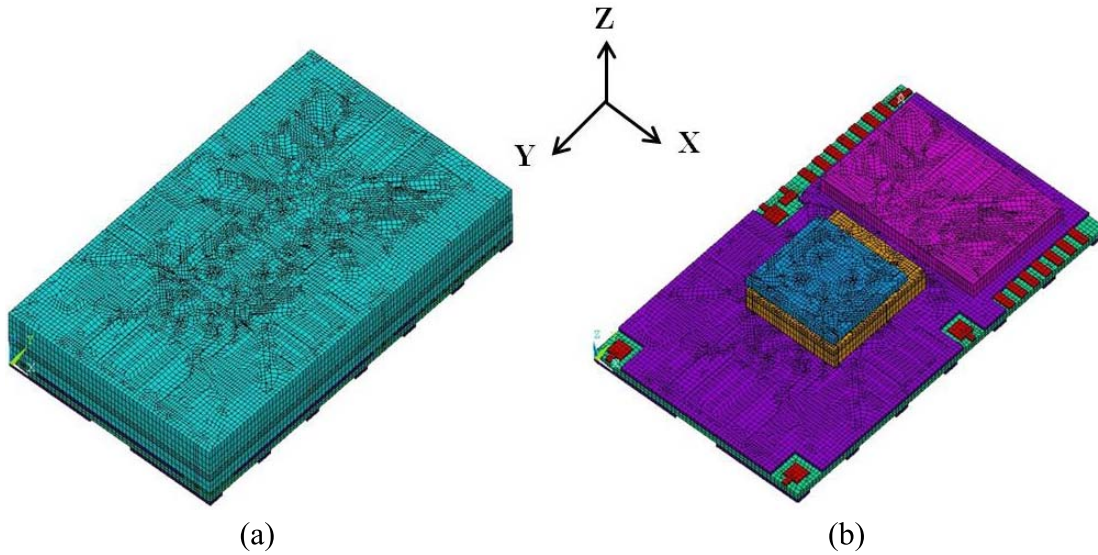


Fig. 10. MEMS sensor device FEA model. (a) MEMS. (b) Inside structure.

the viscoelastic model, the elastic model responds instantly to the temperature change. The warpage of the viscoelastic model is less than that of the elastic model and a decrease of warpage at room temperature is observed due to the time effect. The results imply that the deformation and stress of the MEMS package is overestimated when the only elastic material properties are used for the molding compound. The stress change of sensor die is shown in Fig. 12 with a negative value denoting a compression stress. Unlike the warpage change, the stress at the center of the sensor die surface is almost constant in the temperature range over the stress-free temperature. In addition, it shows a very low value close to zero. This can be attributed to the low modulus of the molding compound over  $T_g$ . In Figs. 4 and 5, the modulus of the molding compound is  $<1$  GPa over  $125$  °C. Although the sensor chip deforms, the low modulus of molding compound in high temperature does not restrict it so that stress does not occur in the sensor die. As observed in Figs. 11 and 12, a significant change of deformation and stress accumulates, when the MEMS package is under the cooling condition. Specifically, most of the stress develops in the range from the PMC temperature to room temperature. Therefore, simulations to minimize the stress of sensor die were performed in this temperature region.

Park *et al.* [12] studied the effect of cooling rate on the stress of MEMS packages. It has been shown that the cooling rate has a great impact on the stress of MEMS packages due to the intrinsic time-dependent features of polymer-based materials such as molding compound (Fig. 13). Slow cooling can reduce the stress generation on the MEMS chip. However, it may be not practical to modify the cooling rate because of the subsequent increase in manufacturing cost and time in the production line. Thus, it is still important to find the optimal material properties of molding compound to minimize the thermally-induced stresses and strains inside the MEMS package.

To predict the viscoelastic behavior accurately, the temperature profile for the cooling process was generated by a transient

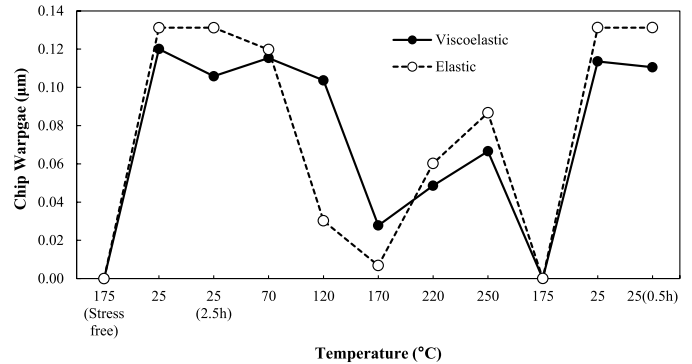


Fig. 11. Warpage history of sensor chip.

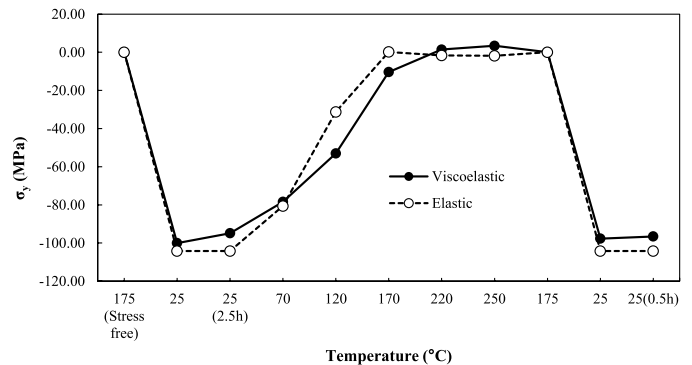


Fig. 12. Stress ( $\sigma_y$ ) history at the center of sensor chip.

heat analysis [12]. If the nonuniformity of the package inside is neglected, the temperature change of MEMS package is expressed by

$$Ah(T - T_\infty) = -\rho Vc \frac{dT}{dt} \quad (5)$$

where  $T_\infty$  is the environmental temperature,  $\rho$  is the density,  $V$  is the volume of the package,  $A$  is the package surface area,  $c$  is the specific heat, and  $h$  is the heat transfer coefficient for

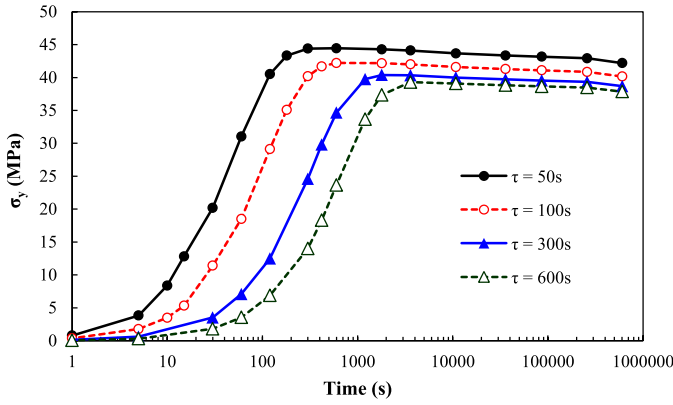


Fig. 13. Stress-time curve effect of different cooling rate on thermal stress [12].

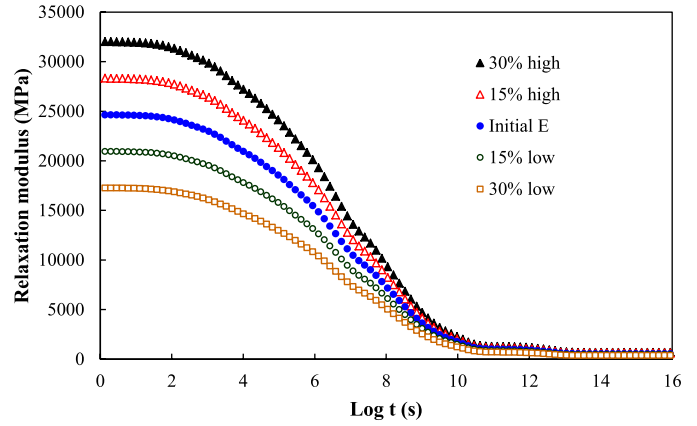


Fig. 15. Master curves by modulus change of molding compound.

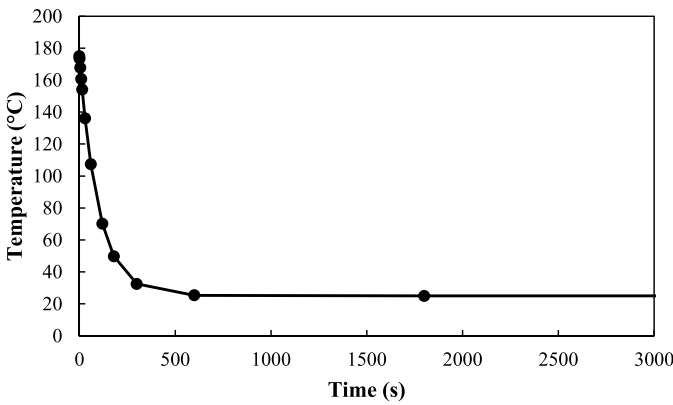


Fig. 14. Temperature profile for the cooling process (PMC to room temperature).

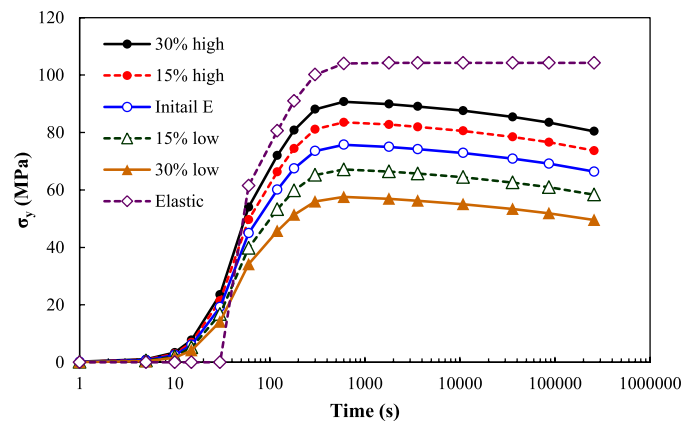


Fig. 16. Modulus effect on the chip stress.

natural convection in air. This equation yields

$$\frac{T - T_\infty}{T_i - T_\infty} = \exp\left(-\frac{t}{\tau}\right), \quad \tau = \frac{\rho V c}{Ah} \quad (6)$$

where  $T_i$  is the initial temperature and  $\tau$  is called time constant. The time constant is independent of temperature. Finally, this equation can be expressed by

$$T = (T_i - T_\infty)\exp\left(-\frac{t}{\tau}\right) + T_\infty. \quad (7)$$

Based on the manufacturing condition,  $\tau$  was assumed to be 100 s. The temperature profile constructed by (7) is shown in Fig. 14. This curve was used for the analysis to optimize the molding compound material properties. The total time simulated was 259 200 s (72 h). The effects of modulus, CTE, and  $T_g$  of molding compound were investigated in this paper. Even though this paper concentrates on the change of a single engineering property of the molding compound, it has to be noted that there are relationships between the many material properties of a molding compound. The major constituents of molding compound are the silica filler and epoxy. Since the silica filler has a much higher modulus and lower CTE than the epoxy, as the amount of silica filler increases, the modulus of the molding compound also goes up. On the other hand, the added filler content makes the CTE decrease. Some works in the literature, notably [13], have proposed expressions of the

total material properties of packaging material as a function of silica filler content and  $T_g$ . The interaction of material properties, however, was not considered in the simulation because there are many epoxy resin systems having different material characteristics and the purpose of this paper is to present the optimal trend of each engineering property to reduce the chip stress.

First of all, the modulus effect was evaluated. The original master curve in Fig. 4 was modified and input to the cooling simulation. Fig. 15 shows the adjusted master curves for this simulation. The result of the cooling simulation is shown in Fig. 16. To observe the effect of time clearly, logarithmic scale was used for the  $x$ -axis. When the package is cooling down, the chip is under compression stresses due to the relatively higher CTE of molding compound and substrate than the chip. Please note that the negative sign denoting compressive stress was removed for convenience in the following results. As shown in Fig. 16, the stress exhibits the maximum when the temperature reaches room temperature (at about 600 s in Fig. 14) and goes slowly down as time passes. Compared with the temperature, the time has much less impact on the stress seen by the chip. The low modulus of molding compound induces less stress on the chip than one with a high modulus. In addition, the temperature-dependent elastic model with no viscoelasticity was also analyzed for comparison. As shown in Fig. 16, the maximum thermal stress from the elastic model

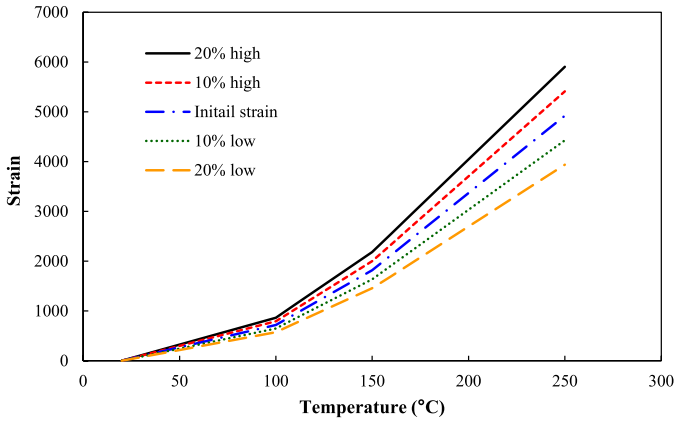


Fig. 17. Thermal strain change (CTE change).

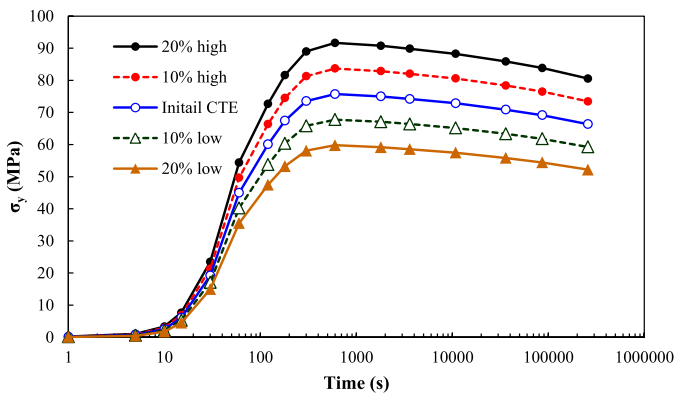
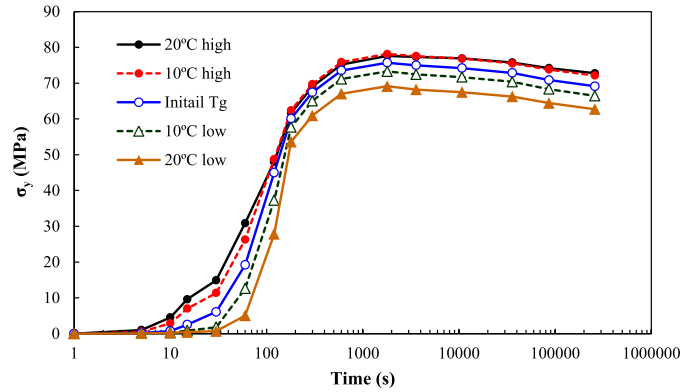


Fig. 18. CTE effect on the chip stress.

(labeled elastic) is about 35% higher than the viscoelastic model (labeled initial E) around 600 s. This significant discrepancy may mislead engineers into overestimation of the thermal stress on the chip.

To see the impact of CTE, the strain from the experiment was also shifted from the experimental data. The thermal strain change for the simulation is shown in Fig. 17. The slope of each curve was used as the CTE for the subsequent simulation. Similarly, the stress plots in Fig. 18 show that the least thermal stress is observed when the molding compound has the lowest CTE. In both cases (Figs. 16 and 18), based on the temperature profile in Fig. 14, the thermal stress is almost zero above  $T_g$  and it increases significantly when the temperature passes  $T_g$  and goes down to the environmental temperature. Therefore, it can be concluded that the modulus and CTE around and under  $T_g$  are key parameters to reduce the thermal stress.

The effect of  $T_g$  was also analyzed. By adding or subtracting a certain value to or from  $x$ -axis (temperature) of the shift function in Fig. 5,  $T_g$  was shifted. In this case, the CTE was also adjusted in accordance with  $T_g$ . The simulation result is shown in Fig. 19. The lowest  $T_g$  generates minimum stress. As mentioned earlier, the modulus of molding compound decreases above  $T_g$ . Accordingly, less thermal stress is developed when the molding compound has a lower  $T_g$ . Contrary to previous results, the stress generation starts at different time due to the different  $T_g$  in Fig. 19. However,

Fig. 19.  $T_g$  effect on the chip stress.

the stress difference between curves after cool down is less than the result of modulus and CTE. Even though the low  $T_g$  material can alleviate the MEMS stress, caution should be exercised when selecting a low  $T_g$  molding compound. The reason for this is because if  $T_g$  is in the operating temperature range of the component, the stress level of chip will keep changing depending on the temperature cooling rate. This will be investigated in more detail in future studies.

## VII. CONCLUSION

An optimization process for the viscoelastic properties of molding compound material for MEMS sensor package has been studied. The FEA was performed to reduce the thermal stress on the MEMS sensor chip. The viscoelasticity of molding compound was characterized and modeled in the FEA. Comparison of the MEMS package warpage between experiment and simulation indicates good accuracy of the simulation results. Results of the process analysis indicate that the majority of the thermal stress is generated during the cooling process. Specifically, the stress development as the component is cooled from the stress free temperature (PMC temperature) to room temperature is significant. It also can be seen that the die stress is close to zero above the PMC temperature. Therefore, the cooling profile from the PMC temperature to room temperature was constructed based on simulation results of a transient heat analysis and was used for the optimization study. The optimization results show that low modulus, low CTE, and low  $T_g$  material properties of molding compound can reduce the stress on the sensor chip. It is also shown that a purely elastic model for molding compound exaggerates the thermal stress in the simulation. For more accurate estimation of the stress, other factors on molding compound, such as cure shrinkage, hygroscopic swelling, and residual stress will be addressed in future studies.

## REFERENCES

- [1] X. Zhang, S. Park, and M. W. Judy, "Accurate assessment of packaging stress effects on MEMS sensors by measurement and sensor-package interaction simulations," *J. Microelectromech. Syst.*, vol. 16, no. 3, pp. 639–649, Jun. 2007.
- [2] R. H. Krondorfer and Y. K. Kim, "Packaging effect on MEMS pressure sensor performance," *IEEE Trans. Compon. Packag. Technol.*, vol. 30, no. 2, pp. 285–293, Jun. 2007.

- [3] M. Amagai, "Characterization of chip scale packaging materials," *Microelectron. Rel.*, vol. 39, no. 9, pp. 1365-1377, 1999.
- [4] N. Srikanth, "Warpage analysis of epoxy molded packages using viscoelastic based model," *J. Mater. Sci.*, vol. 41, no. 12, pp. 3773-3780, 2006.
- [5] M.-Y. Tsai, C. T. Wang, and C. H. Hsu, "The effect of epoxy molding compound on thermal/residual deformations and stresses in IC packages during manufacturing process," *IEEE Trans. Compon. Packag. Technol.*, vol. 29, no. 3, pp. 625-635, Sep. 2006.
- [6] P. Alpern *et al.*, "On the way to zero defect of plastic-encapsulated electronic power devices—Part II: Molding compound," *IEEE Trans. Device Mater. Rel.*, vol. 9, no. 2, pp. 279-287, Jun. 2009.
- [7] S.-H. Chae, J.-H. Zhao, D. R. Edwards, and P. S. Ho, "Characterization of the viscoelasticity of molding compounds in the time domain," *J. Electron. Mater.*, vol. 39, no. 4, pp. 419-425, 2010.
- [8] R. Krondorfer, Y. K. Kim, J. Kim, C.-G. Gustafson, and T. C. Lommasson, "Finite element simulation of package stress in transfer molded MEMS pressure sensors," *Microelectron. Rel.*, vol. 44, no. 12, pp. 1995-2002, 2004.
- [9] J.-W. Joo and S.-H. Choa, "Deformation behavior of MEMS gyroscope sensor package subjected to temperature change," *IEEE Trans. Compon. Packag. Technol.*, vol. 30, no. 2, pp. 346-354, Jun. 2007.
- [10] Y. Kim, H. Lee, X. Zhang, and S. Park, "Stress relaxation test of molding compound for MEMS packaging," in *Proc. 13th IEEE Inter-soc. Conf. Thermal Thermomech. Phenomena Electron. Syst. (ITherm)*, May/June. 2012, pp. 290-296.
- [11] S. Imaoka. (2008). *Sheldon's ANSYS Tips on Viscoelasticity*. [Online]. Available: <http://ansys.net>
- [12] S. Park, D. Liu, Y. Kim, H. Lee, and X. Zhang, "Stress evolution in an encapsulated MEMS package due to viscoelasticity of packaging materials," in *Proc. IEEE 62nd Electron. Compon. Technol. Conf. (ECTC)*, May/June. 2012, pp. 70-75.
- [13] J. M. Hurley, "Estimating the engineering properties of electronic packaging materials," *IEEE Trans. Compon. Packag. Technol.*, vol. 31, no. 2, pp. 417-424, Jun. 2008.
- [14] H.-J. Tai and H.-L. Chou, "Chemical shrinkage and diffusion-controlled reaction of an epoxy molding compound," *Eur. Polymer J.*, vol. 36, no. 10, pp. 2213-2219, Oct. 2000.
- [15] S. Park, R. Dhakal, and R. Joshi, "Comparative analysis of BGA deformations and strains using digital image correlation and Moiré interferometry," in *Proc. Annu. Conf. Soc. Experimental Mech.*, Portland, OR, USA, Jun. 2005, pp. 1-8.



**Yeonsung Kim** received the B.S. and M.S. degrees in mechanical engineering from Chung-Ang University, Seoul, Korea, in 2002 and 2004, respectively, and the Ph.D. degree in mechanical engineering from the State University of New York at Binghamton, Binghamton, NY, USA, in 2014.

He joined Samsung Electronics Company, Ltd., Suwon, Korea, in 2004, where he was involved in evaluating and improving a reliability of electronic packaging for mobile devices for four and a half years. He is currently a Packaging and Assembly

Engineer with Analog Devices, Inc., Wilmington, MA, USA, where he is involved in packaging development for microelectromechanical systems.



**Hohyung Lee** received the B.S. degree in industrial system engineering and the M.S. degree in mechanical engineering from the State University of New York at Binghamton, Binghamton, NY, USA, where he is currently pursuing the Ph.D. degree with the Opto-Mechanics and Physical Reliability Laboratory, Department of Mechanical Engineering.



**Xin Zhang** received the B.S. degree from Tsinghua University, Beijing, China, and the M.S. degree from George Washington University, Washington, DC, USA.

He joined Analog Devices, Inc. (ADI), Wilmington, MA, USA, in 2001. He designed ADI's 1st 3-axis accelerometer and then a series of 3-axis accelerometer products for industrial, consumer, and automotive applications. He also designed ADI's first microelectromechanical systems (MEMS) microphone product and the

first highest performance 66-dB SNR microphone products. He is currently a Senior Staff MEMS Design Engineer with the MEMS and Sensors Core Products & Technologies Division, ADI. He is currently involved in high-performance inertial sensors (accelerometers and gyroscopes) design and simulation. He has also done extensive research in packaging material and stress characterization and modeling. His work has resulted in numerous ADI internal and international product awards. He holds over 20 issued patents.



**Seungbae Park** received the Ph.D. degree from Purdue University, West Lafayette, IN, USA, in 1994.

He was with IBM, Armonk, NY, USA, as a Development and Reliability Engineer, where he was responsible for flip-chip technology. Since 2002, he has been a Professor with the Department of Mechanical Engineering, State University of New York at Binghamton, Binghamton, NY, USA. He has authored over 100 technical publications, and holds four U.S. patents. His current research interests

include physical reliability for microelectronics and microelectromechanical systems packaging.

Dr. Park has served many technical communities. He was Chair of the iNEMI's Modeling and Simulation Technical Work Group and the Electronics Packaging Council in the Society of Experimental Mechanics. He was also a Reliability Committee Member of the Electronic Components and Technology Conference and the American Society of Mechanical Engineers.